Supplemental Information

Observations of Volatile Organic Compounds in the Los Angeles Basin during COVID-19

Paul Van Rooy,[†] Afsara Tasnia, [†,‡] Barbara Barletta, [§] Reina Buenconsejo, [‖] John D. Crounse, [‖,b] Christopher Kenseth, [‖] Simone Meinardi, [§] Sara Murphy,[a] Harrison Parker,[a] Benjamin Schulze, [a] John H. Seinfeld, [a,b] Paul O. Wennberg, [a,b] Donald R. Blake, [§] and Kelley C. Barsanti[*,†,‡]*

[†]Bourns College of Engineering, Center for Environmental Research and Technology, Riverside, CA, 92507, USA

[‡]Department of Chemical and Environmental Engineering, University of California, Riverside, CA, 92507, USA

[§]Department of Chemistry, University of California, Irvine, CA, 92697, USA

[‖]Division of Chemistry and Chemical Engineering, California Institute of Technology, Pasadena, CA, 91125, USA

[a]Division of Geological and Planetary Sciences, California Institute of Technology, Pasadena, CA, 91125, USA

[b]Division of Engineering and Applied Science, California Institute of Technology, Pasadena, CA, 91125, USA

Index of Figures

S.1 Chemical and Meteorological Comparisons between 2010 and 2020

NO_x data presented in Parker et al.,[1] obtained from 15 South Coast Air Quality Management District air monitoring stations across the LA Basin, were used to calculate the change in NO_x levels between 2010 and 2020 during the period of 15 April to 15 July. The data are presented in Figure S.1. On average, NO_x levels decreased by 49% between 2010 and 2020. In addition, NO_x data from the California Air Resources Board monitoring station in Pasadena (South Wilson) were used to calculate the change in NO_x levels between 2010 and 2020; an approximate 50% decrease in NO_x was calculated using these data.

Wind speed and direction during daytime and nighttime sampling periods in April, May, June, and July 2020 and daytime sampling periods during April-July in 2010 and 2020 are shown in Figures S.2-S.4. Morning wind was generally stagnant (0-3 m/s), while afternoon wind was 3-5 m/s from the southwest. Wind speed in 2020 is qualitatively similar to 2010, particularly during the afternoon sampling periods when wind speeds were between 3-5 m/s, suggesting transport times and trajectories were similar. Afternoon airmass back trajectories (Figure S.5) starting at 14:00 local time were calculated using the Hybrid Single-Particle Lagrangian Integrated Trajectory (HYSPLIT) model[2] at an altitude of 250 m on Wednesday for each week of the campaign. Meteorological data at a resolution of 12 km x 12 km were obtained from the

North American Mesoscale Forecast System (NAMS) archive

(https://ready.arl.noaa.gov/archives.php).

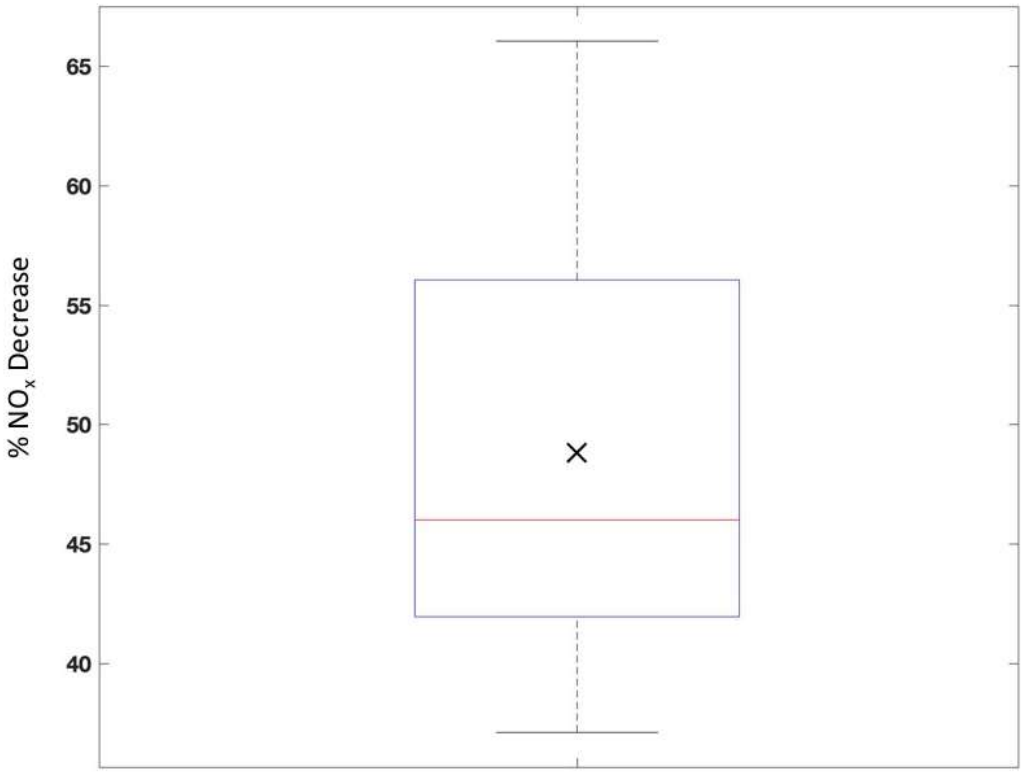

Figure S.1. Boxplot showing the range of % NO_x decreases in the LA Basin between 2010 and 2020, measured across 15 stations during 15 April to 15 July. The median is represented by the red line, the 25th and 75th percentiles by the edges of the blue box, and the mean by a black '×'.

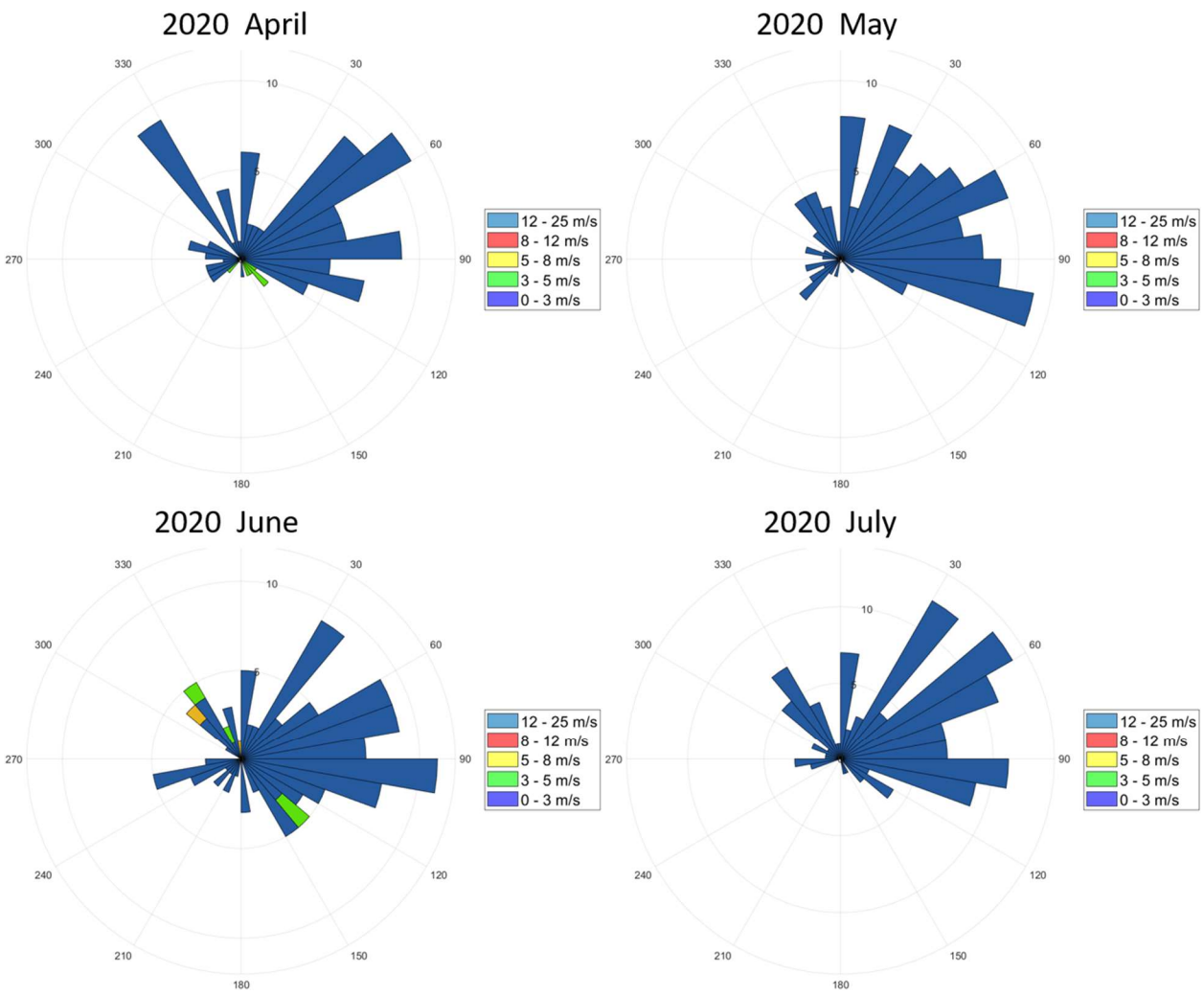

Figure S.2. Wind direction and speed recorded at 05:30-06:30 in April, May, Jun, and July during the LAAQC-2020 campaign. Wind data were from the NOAA integrated surface database.

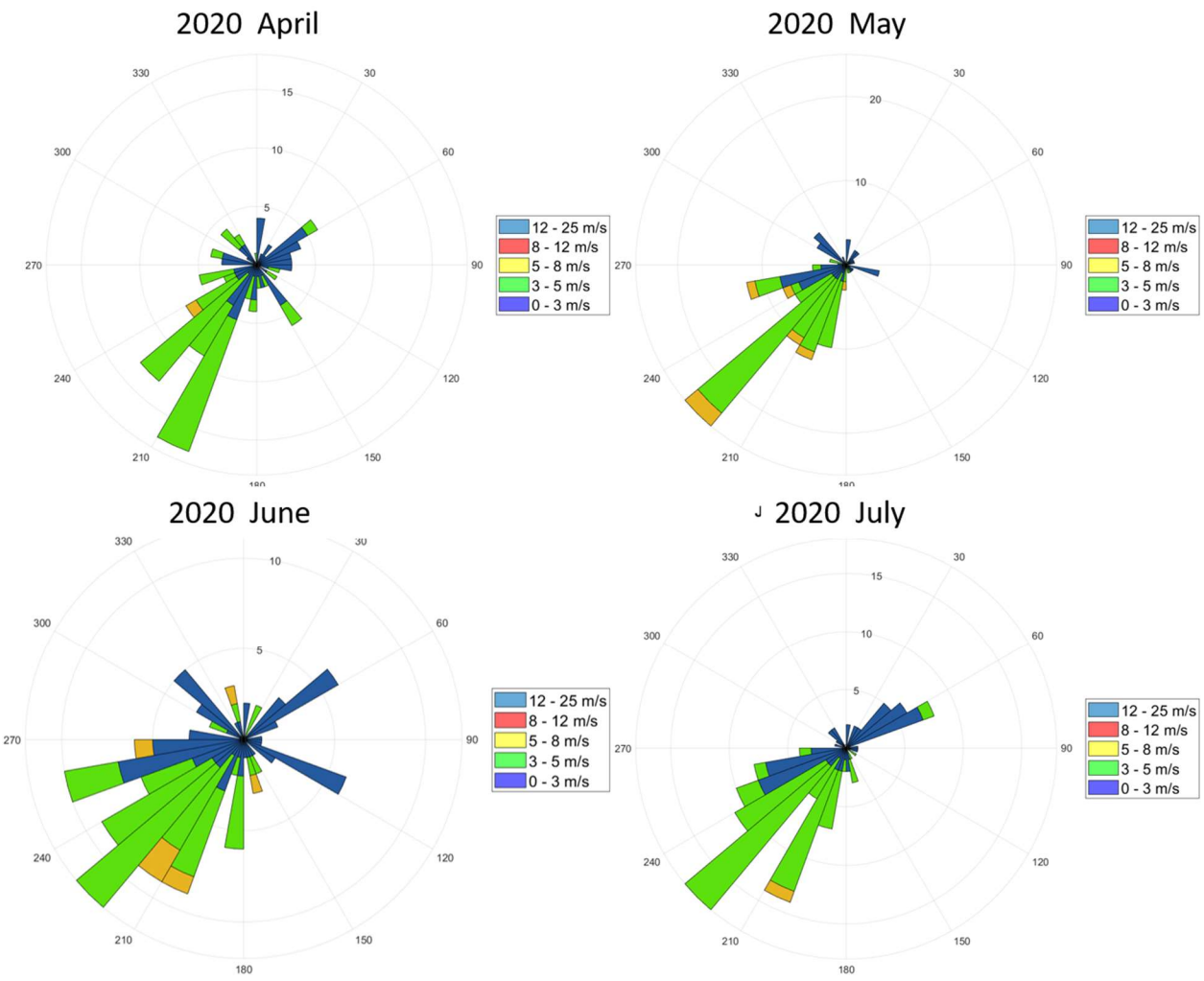

Figure S.3. Wind direction and speed recorded at 14:00-15:00 in April, May, Jun, and July during the LAAQC-2020 campaign. Wind data were from the NOAA integrated surface database.

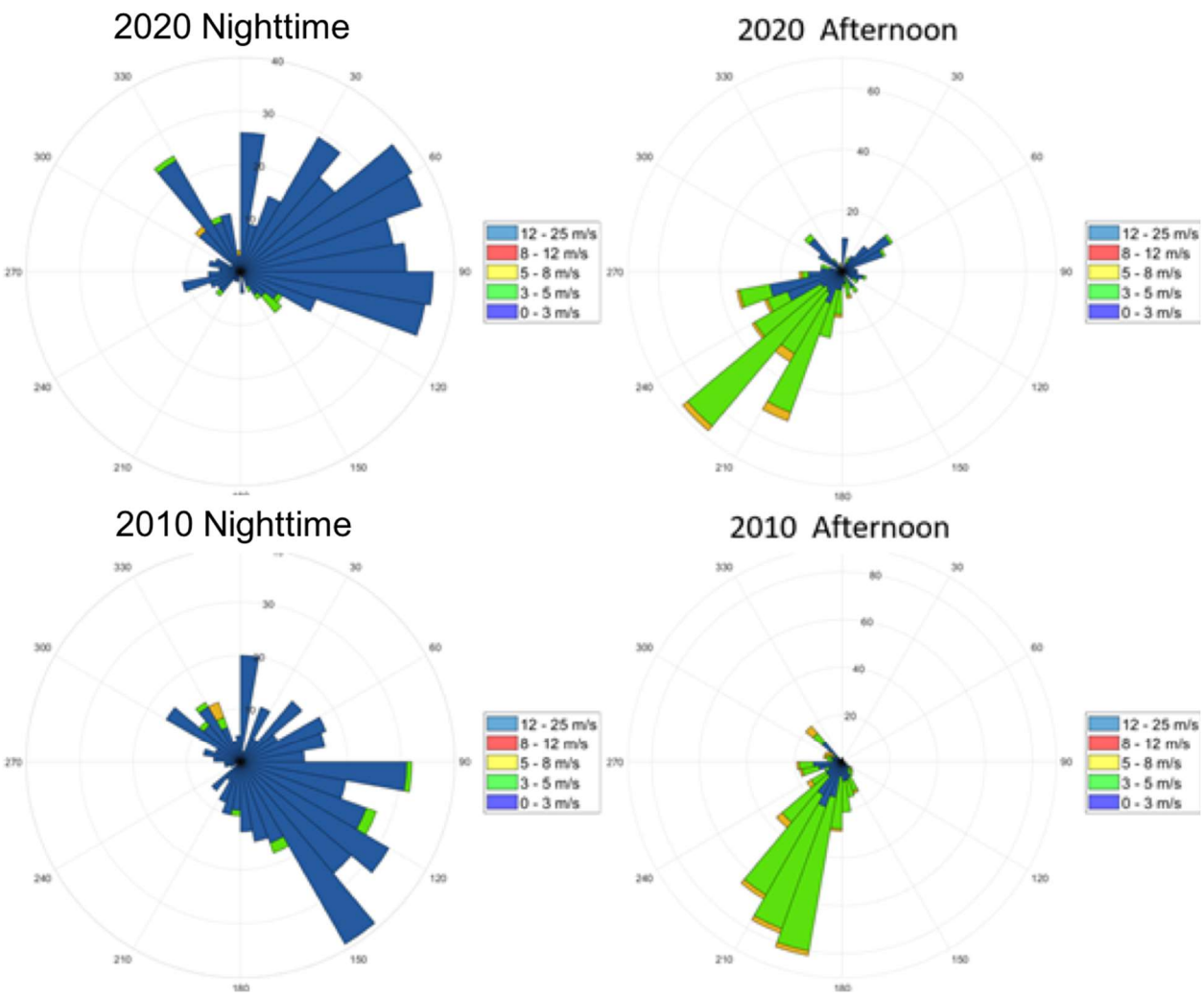

Figure S.4. Wind direction and speed recorded at 05:30-06:30 and 14:00-15:00 in April-July during 2020 and 2010. Wind data were from the NOAA integrated surface database.

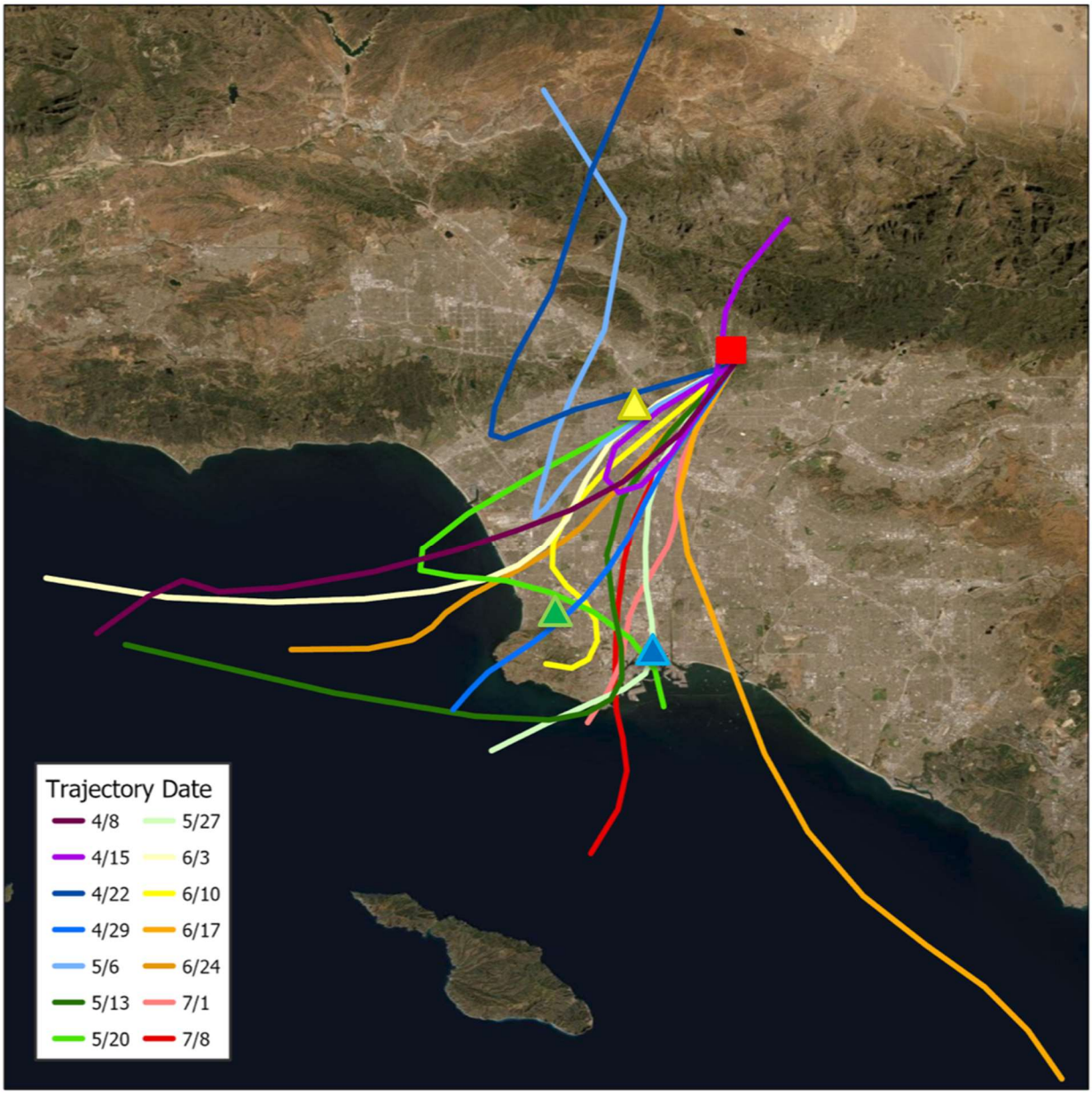

Figure S.5. Afternoon airmass back trajectories for each week of LAAQC-2020 calculated using Hybrid Single-Particle Lagrangian Integrated Trajectory (HYSPLIT). Symbols are used to approximate sampling area and source regions: Pasadena (red square), Los Angeles (yellow triangle), Torrance (green triangle), and Long Beach (blue triangle).

S.2 Comparison of VOC mixing ratios quantified by UCI and UCR

During LAAQC nine compounds (decane, octane, nonane, 2-methylpentane, 2,3-dimethylpentane, ethylbenzene, o-xylene, m+p-xylene, and toluene) were quantified by both

UCR and UCI. A total of 1170 paired (9 × # of samples collected at the same date and time by UCI and UCR) VOC measurements were collected. Figure S.6 shows the extent of agreement, represented as % difference, between UCI and UCR paired VOC measurements, where $\%\ \text{difference} = 100\% \times \frac{|\text{UCI}-\text{UCR}|}{\left|\frac{\text{UCI}+\text{UCR}}{2}\right|}$. Good agreement was observed for a majority of the paired VOC measurements: over half, 58%, agreed within 25% and 84% agreed within 50%. Potential reasons for disagreement outside the uncertainty limits of the methods include influence of highly localized sources: samplers were co-located ~15 feet apart, but had different orientations with one inlet on the south side of the building and one inlet on the east side of the building; and oxidation: UCR uses a pre-filter to scrub O_3 whereas UCI does not. Comparisons of individual compounds are shown in Figures S.7-S.15.

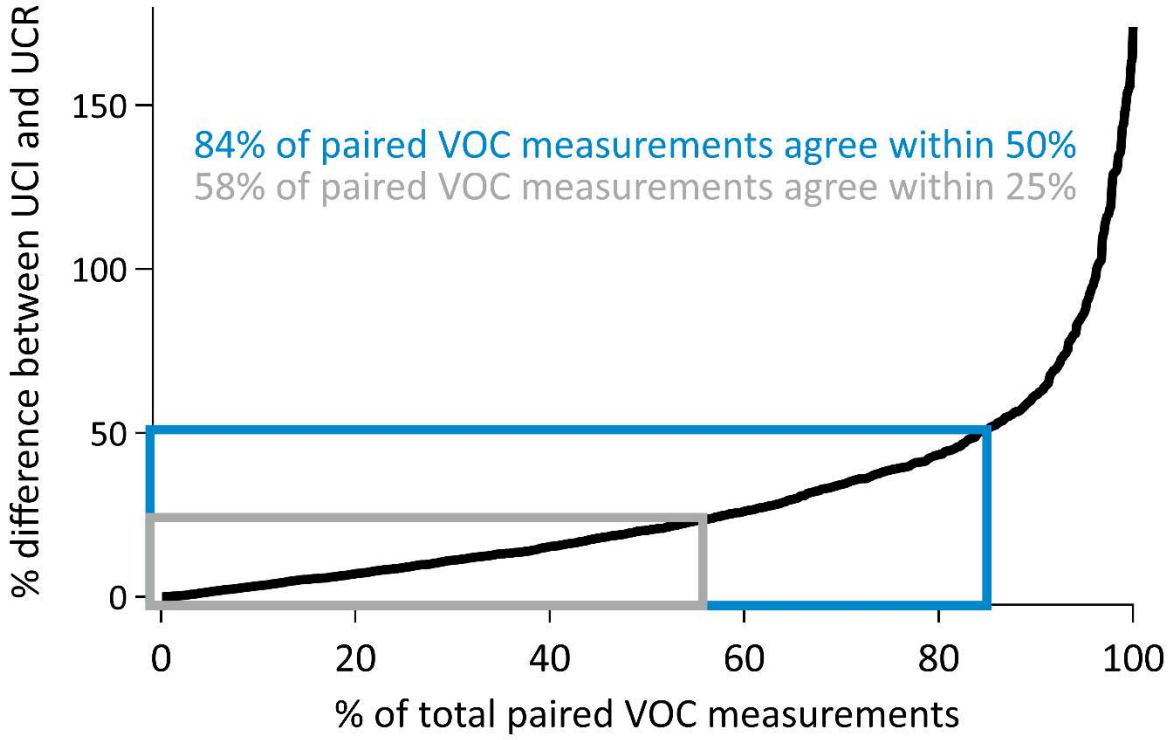

Figure S.6. Percent difference between UCI and UCR mixing ratios plotted against the percentage of paired VOC measurements that fall within the percent difference. The grey square indicates the

percentage of UCI and UCR paired VOC measurements that agree within 25%; the blue square indicates the percentage of paired VOC measurements that agree within 50%.

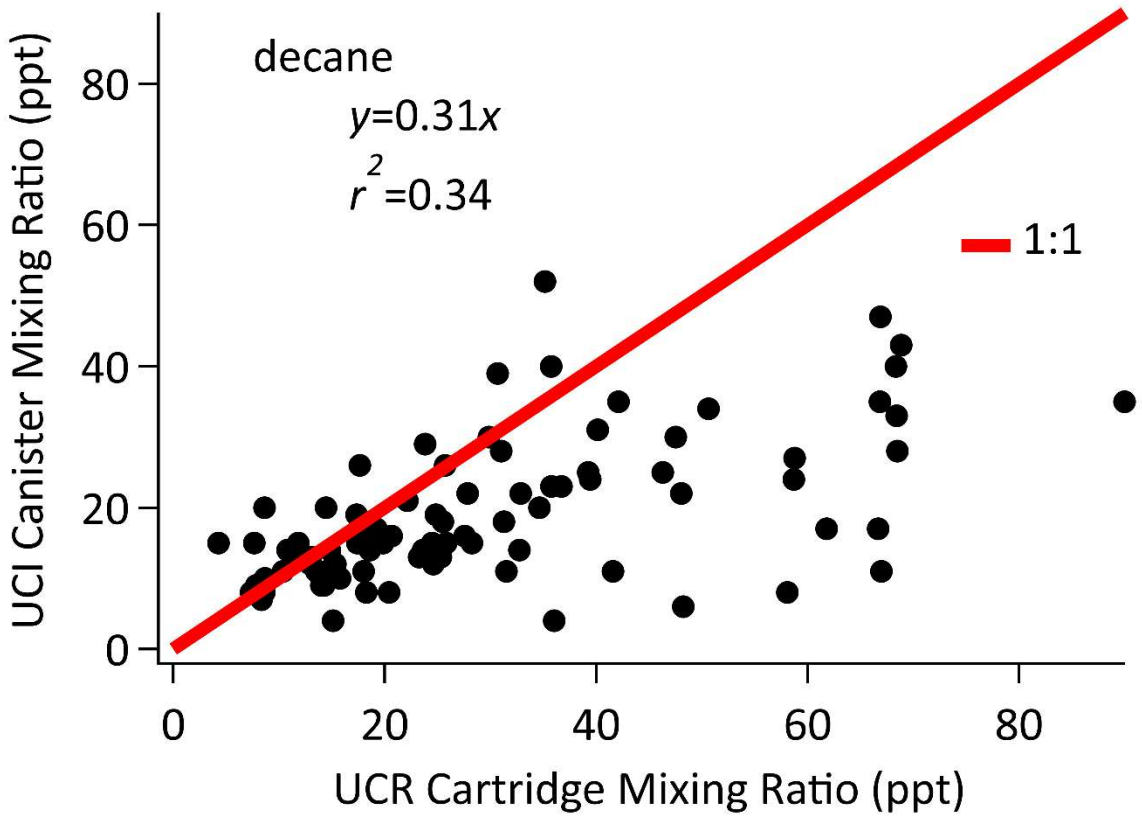

Figure S.7. Measured UCI vs. UCR mixing ratios for decane.

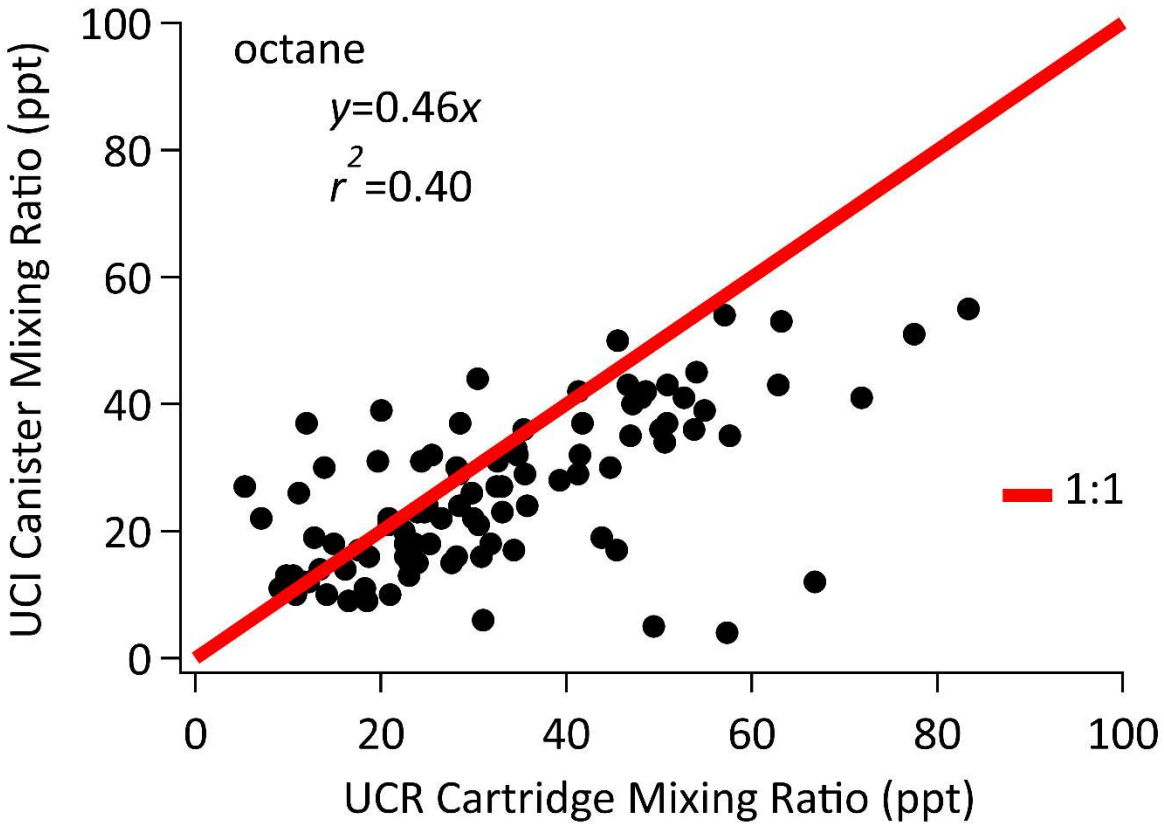

Figure S.8. Measured UCI vs. UCR mixing ratios for octane.

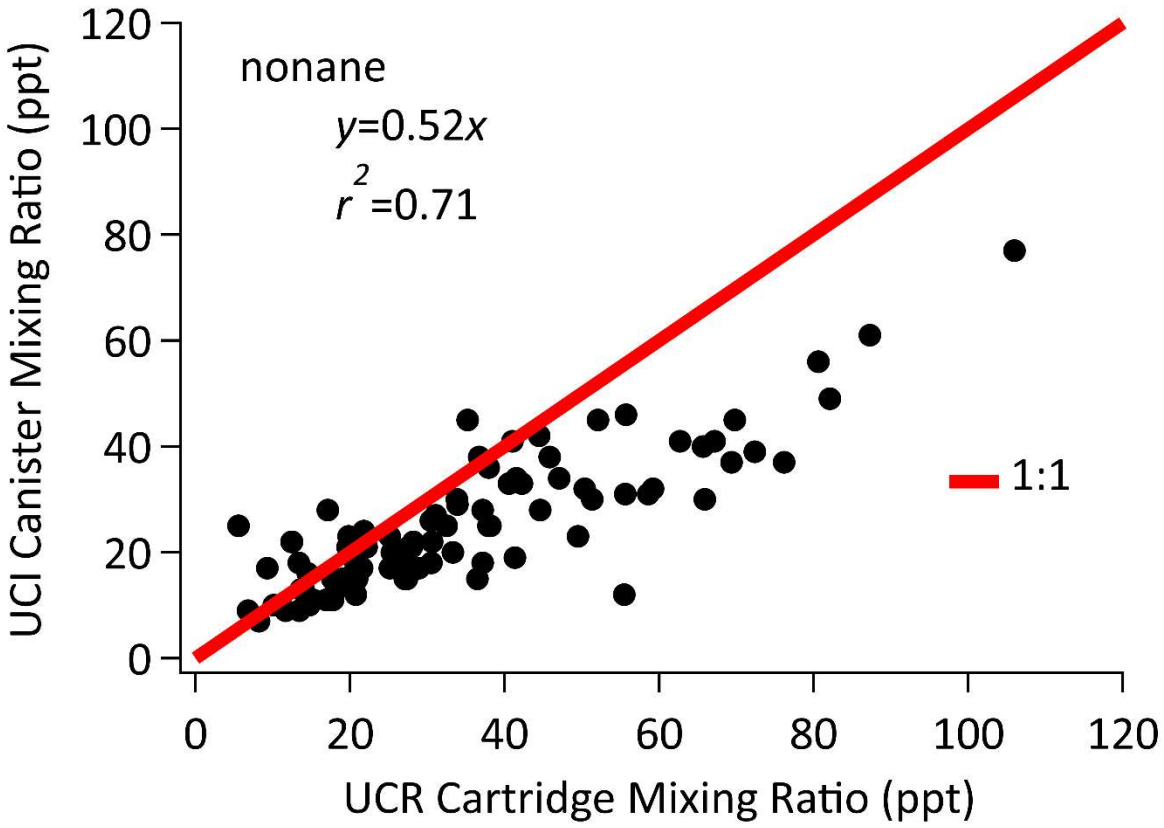

Figure S.9. Measured UCI vs. UCR mixing ratios for nonane.

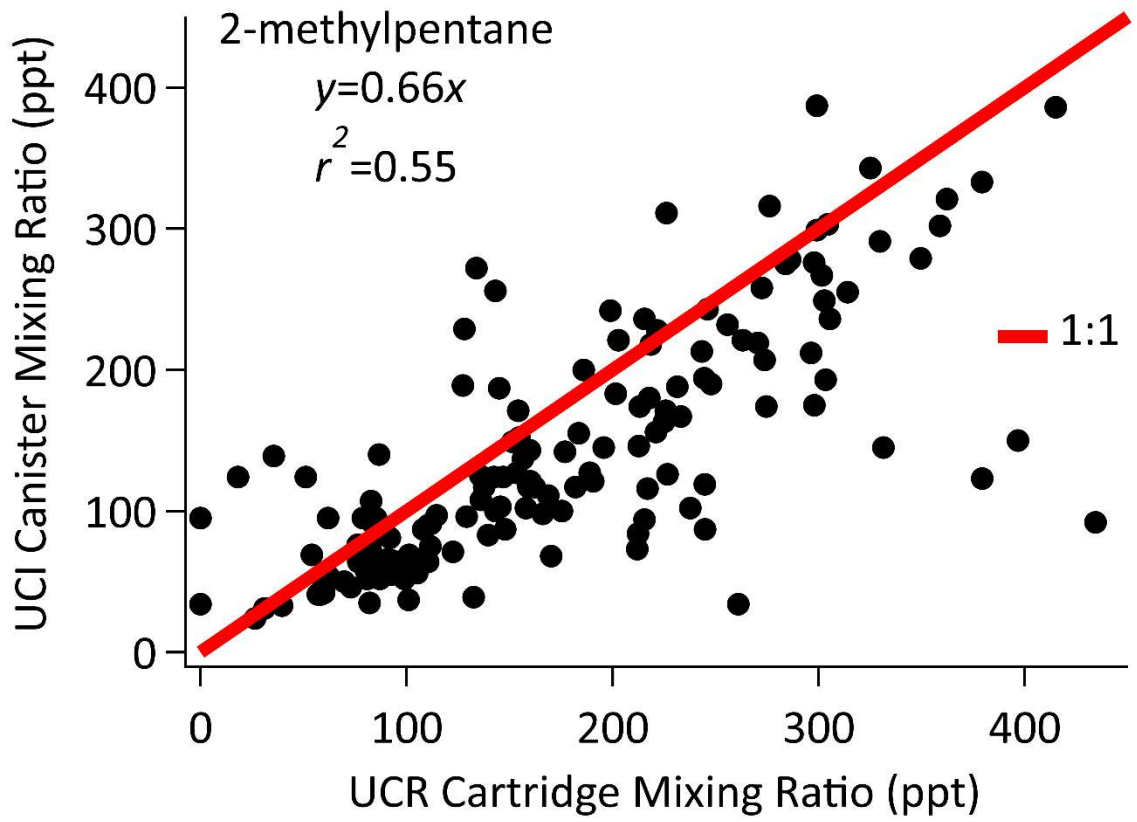

Figure S.10. Measured UCI vs. UCR mixing ratios for 2-methylpentane.

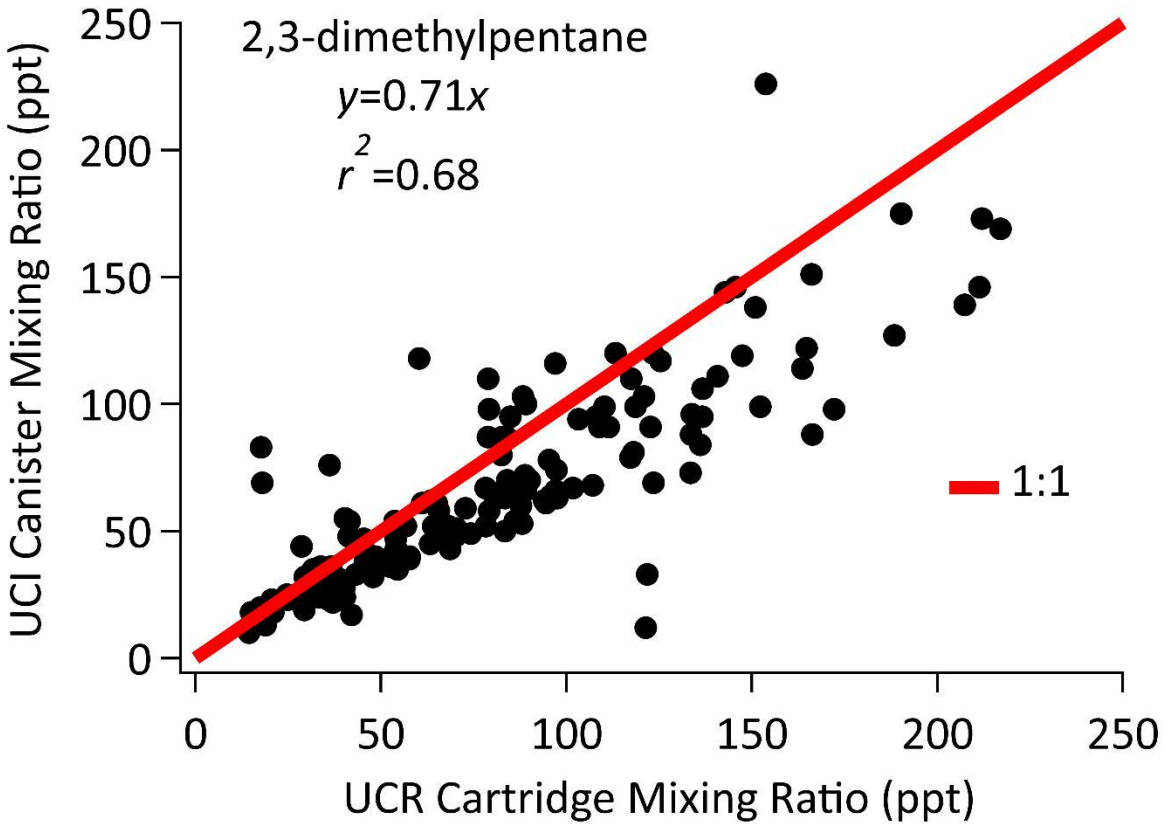

Figure S.11. Measured UCI vs. UCR mixing ratios for 2,3-dimethylpentane.

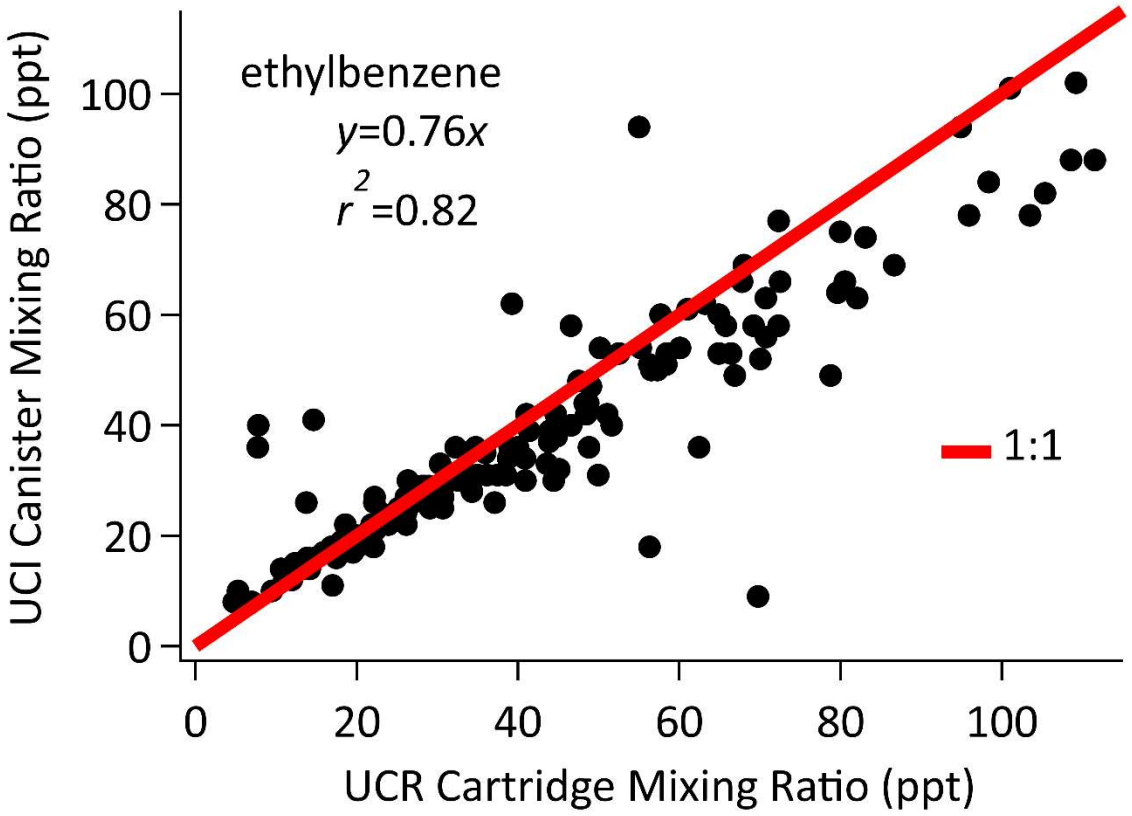

Figure S.12. Measured UCI vs. UCR mixing ratios for ethylbenzene.

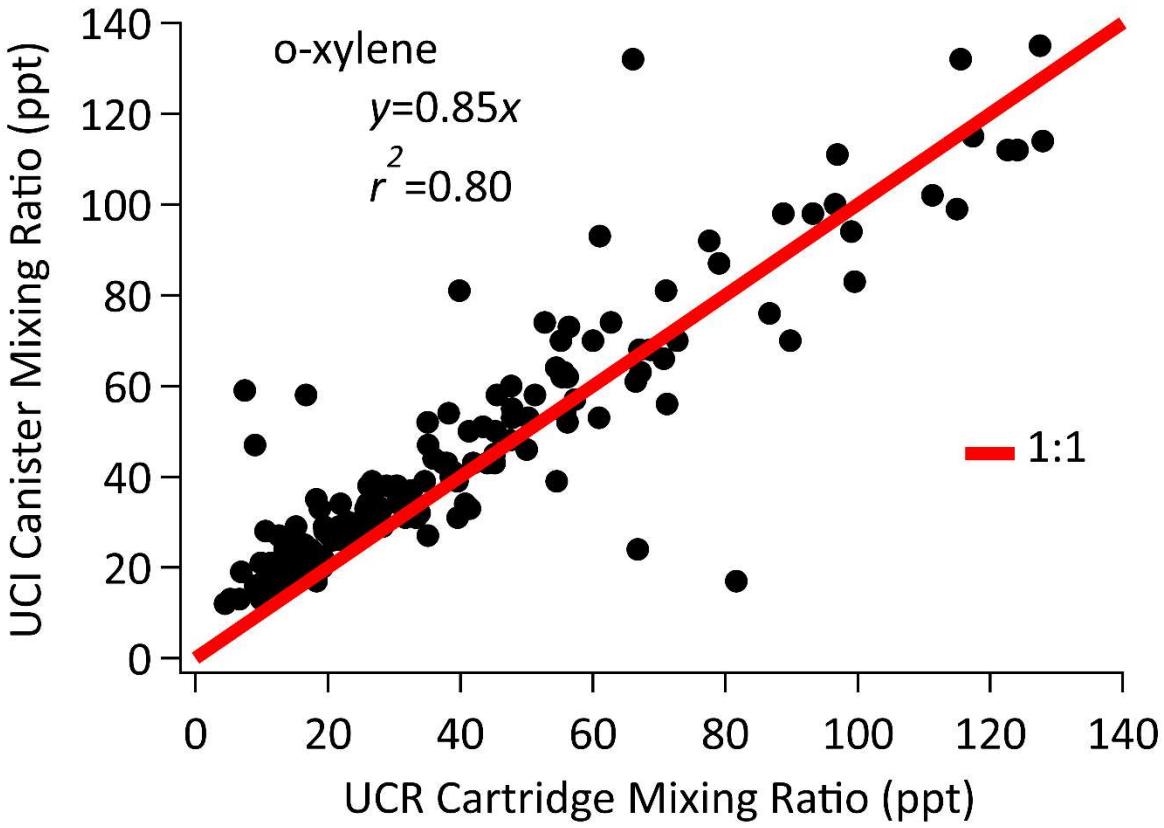

Figure S.13. Measured UCI vs. UCR mixing ratios for o-xylene.

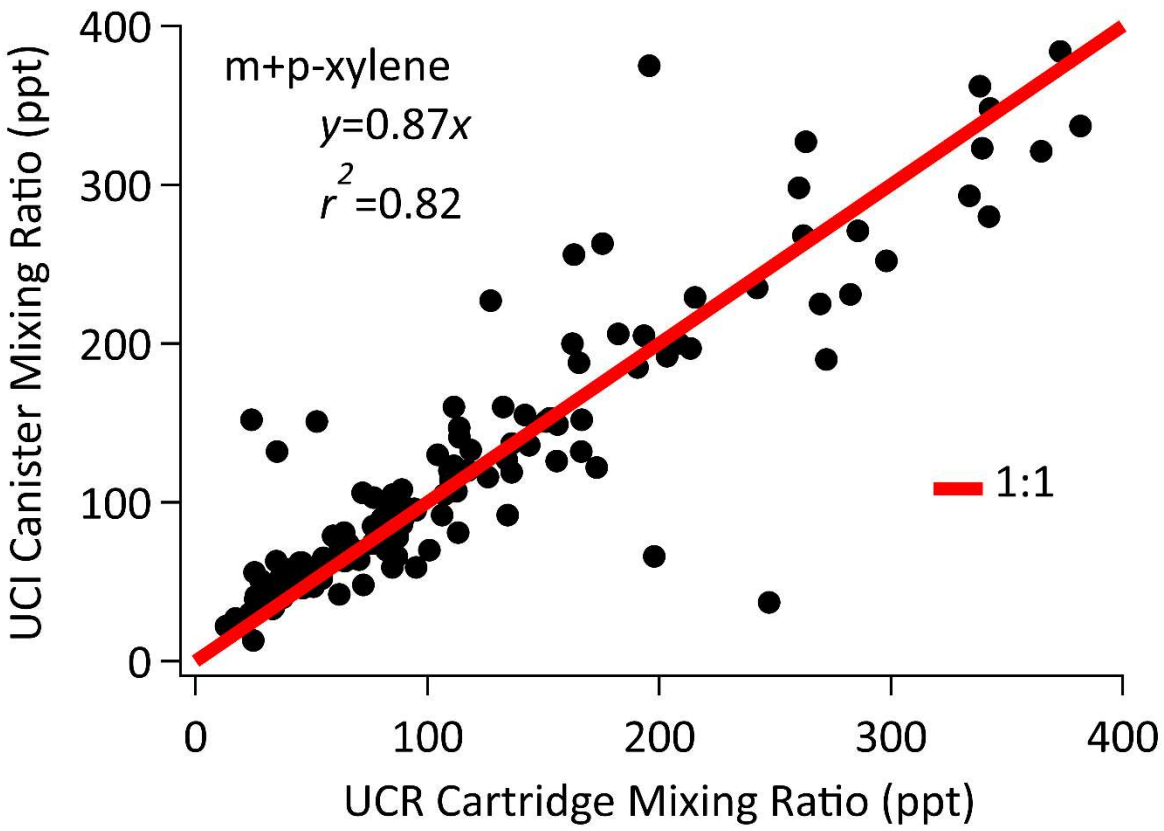

Figure S.14. Measured UCI vs. UCR mixing ratios for m- and p-xylene.

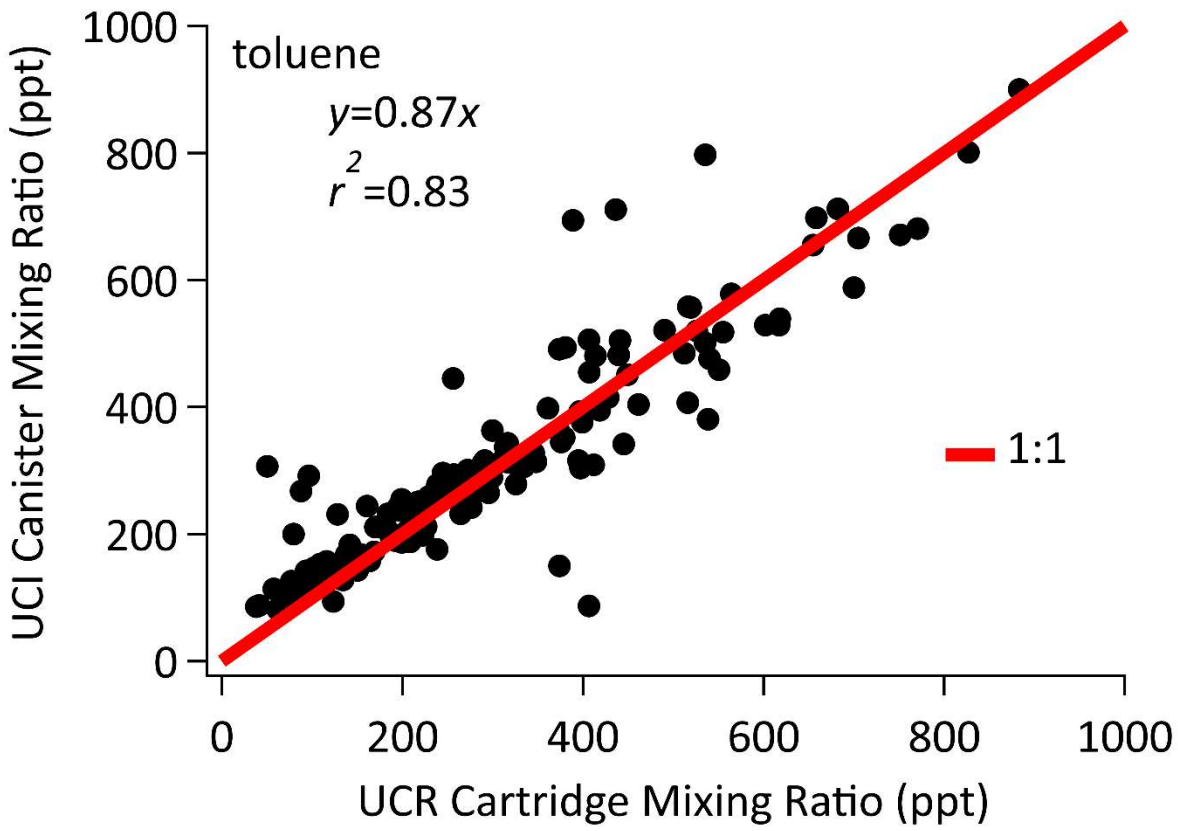

Figure S.15. Measured UCI vs. UCR mixing ratios for toluene.

S.3 Background CO and VOC Calculations

Background-corrected CO values were used in a subset of the ER calculations, as described in the main text. Background CO values were calculated following the approach of de Gouw et al. 2017.[3] First, the CO intercepts of 59 compounds were plotted against their OH reaction rate coefficient, k_{OH} (Figure S.16).[4] The CO intercept of each compound was found from the linear regression of the nighttime mixing ratios of each VOC against the CO mixing ratios. Then, the CO intercepts of m- and p-xylenes (101 ppb), 1,2,4-trimethylbenzene (124-TMB, 84.5 ppb) and 1,3,5-trimethylbenzene (135-TMB, 85.0 ppb) were averaged yielding a background CO value of ~90 ppb. The majority of the CO intercepts fall within +/- 15 ppb of the calculated average, which is therefore defined as the uncertainty in the calculated background CO value. Background CO values calculated at shorter time intervals (monthly) were within the uncertainty (+/- 15 ppb) of the calculated average and did not monotonically increase or decrease during the measurement period. Thus, a constant background CO value of 90 ppb was used in the ER calculations. The background CO mixing ratio was subtracted from the measured CO mixing ratio where noted, ΔCO, and used in the ER calculations. The CO levels during the measurement campaign were not impacted by fires (see Figure S.17) and thus no other CO corrections were applied.

Similarly to CO, VOCs with low OH-reactivity can build up in the atmosphere, affecting ER calculations and source attribution. Five compounds (acetylene, propane, i-butane, n-butane and benzene) with low OH reactivity ($k_{OH} < 5 \times 10^{-12}$ cm^3 molecule^{-1} s^{-1}) had non-negligible background levels. For each of the five compounds, the background VOC mixing ratio was defined as the lowest value. Two benzene and one acetylene values were omitted in determination of the background values as they were anomalously low (>40% lower than the

average of the lowest 2% of mixing ratios). The background mixing ratios for these five compounds were subtracted from the measured mixing ratios and the background-corrected mixing ratios were used in the ER calculations.

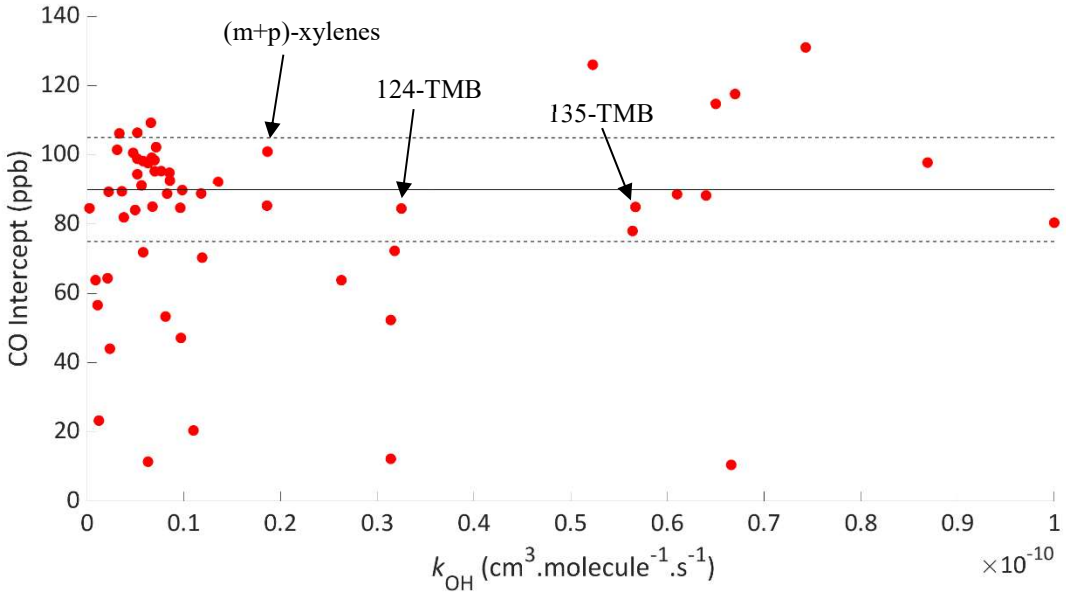

Figure S.16. Calculated CO intercepts for 59 individual VOCs plotted against their OH rate constant[3] for each specific VOC. The solid black line indicates the calculated value for background CO (90 ppb); the two dashed lines indicate +/- 15 ppb.

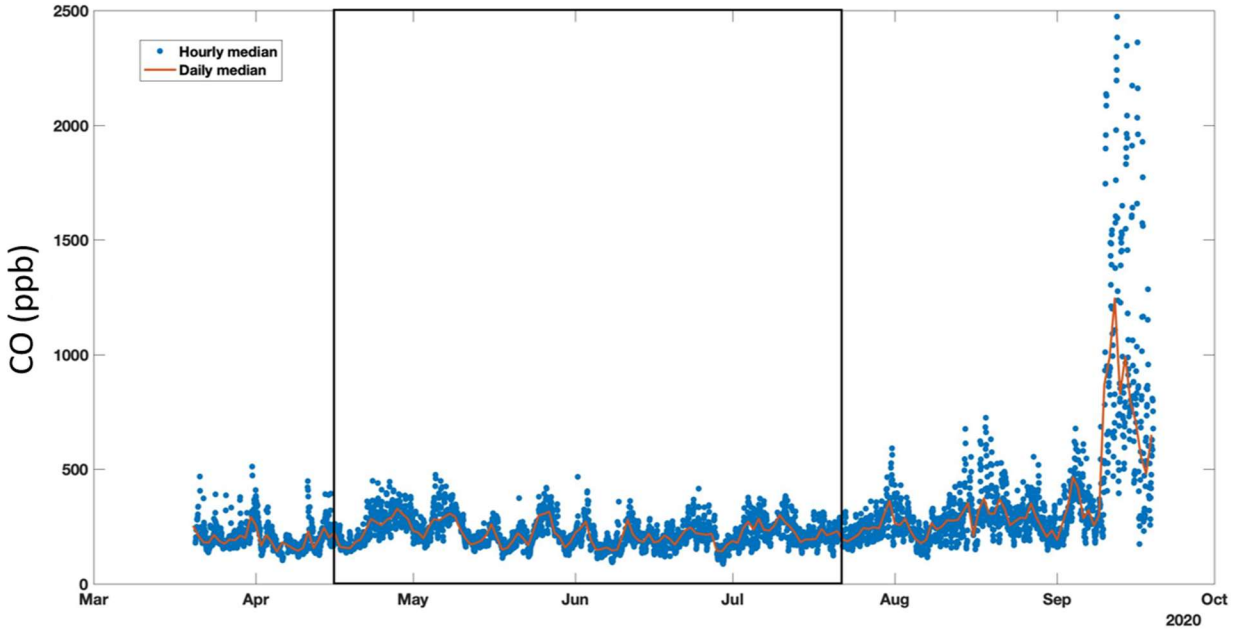

Figure S.17. Hourly median (blue dots) and daily median (orange line) CO mixing ratios measured on the Caltech campus (CITAQS) before, during, and after LAAQC. Dates during the campaign are within the black square.

S.4 Emission Ratio Calculations

Three different ERs relative to CO and acetylene were calculated: nighttime ERs (ER_{night}), OH-corrected ERs, and O_3-corrected ERs_{night}. Nighttime ERs were calculated using nighttime data only (e.g., Borbon et al.[5]). VOC mixing ratios were plotted against CO and the ER was defined as the slope of the linear best fit. This approach was also used to calculate ERs against acetylene. Morning and afternoon sample data cannot be used to calculate ERs by this simple regression method, because OH exposure decreases the levels of reactive VOCs in these samples, resulting in artificially low ERs. de Gouw et al.[3] presented a method for OH-corrected ERs, in which all data can be used following an OH-loss correction. OH exposure can be calculated using the ratio of a less reactive VOC with OH to a more reactive VOC with OH.[6] Following de Gouw et al.,[3] benzene was chosen as the less reactive compound and 11 other

VOCs were evaluated as the more reactive compound. The results of calculated OH exposure using the ratio of benzene to each of these 11 VOCs are shown in Figure S.18. The point markers in Fig. S.18 represent the average OH exposure calculated from the 3×/day samples (05:30–06:30, 09:00–10:00 and 14:00–15:00 PDT) and the lines represent the average OH exposure calculated from two diurnals (one sample per hour over a 24-hr period) that were collected during the campaign.

The ratio of benzene to 1,2,4-trimethylbenzene (yellow trace) was used in Equation S.1 to calculate OH exposure. It represents the average of the 11 pairs and facilitates comparison with de Gouw et al.[3] in which 1,2,4-trimethylbenzene was also used for calculating OH exposure.

$$[\mathrm{OH}]\Delta t = (k_{124\mathrm{TMB+OH}} - k_{\mathrm{benzene+OH}})^{-1} \times \left(\ln\left(\frac{\mathrm{benzene}}{124\mathrm{TMB}}\right) - \ln\left(\mathrm{ER}_{\mathrm{benzene}/124\mathrm{TMB}}\right)\right) \quad \text{(Eq. S.1)}$$

where $\mathrm{ER}_{\mathrm{benzene}/124\mathrm{TMB}}$ is the emission ratio of benzene to 1,2,4-trimethylbenzene and is assumed to be constant across the basin.[3,7] The value of $\mathrm{ER}_{\mathrm{benzene}/124\mathrm{TMB}}$, 1.84, was determined as described below.

$\mathrm{ER}_{\mathrm{benzene}/124\mathrm{TMB}}$ was calculated using two approaches. In the first, a time series of the ratio of the measured mixing ratios was plotted (Figure S.19, top) and the lowest observed ratio is taken as $\mathrm{ER}_{\mathrm{benzene}/124\mathrm{TMB}}$; this approach yielded a value of 1.84. In the second, benzene mixing ratios were plotted against the 1,2,4-trimethylbenzene mixing ratios (Figure S.19, bottom). The $\mathrm{ER}_{\mathrm{benzene}/124\mathrm{TMB}}$ is then defined as the slope of the best linear fit through the least processed air mass, the nighttime samples; this approach yielded a value of 2.1. The lower of the two values, 1.84, was used in the OH exposure calculations. A value of 1.75 ± 0.15 was estimated by de Gouw et al.[3] for CalNex-2010 using the same approach.

Analogous to the OH-corrected ERs calculated from estimated OH exposure, nighttime O_3-corrected ERs were calculated from estimated O_3 exposure (Equation S.2).[3]

$$[O3]\Delta t = (k_{c2But+O3} - k_{benzene+O})^{-1} \times \left(\ln\left(\frac{benzene}{c2But}\right) - \ln\left(ER_{benzene/c2But}\right)\right) \quad \text{(Equation S.2)}$$

Similarly to $ER_{benzene/1,2,4\text{-}trimethylbenzene}$, $ER_{benzene/c2But}$ was calculated using two approaches: 1) plotting the time series of the ratio of the measured mixing ratios; the lowest observed ratio yielded a value of 6.64; and 2) plotting benzene mixing ratios against cis-2-butene mixing ratios from nighttime samples only; the best linear fit yielded a slope of 7. The lowest value, 6.64, was used in Equation S1 for calculating O_3 exposure. de Gouw et al.[3] estimated a value of 5±2 using the same approach. Using the nighttime data only, VOC/CO ratios were plotted against the corresponding O_3-exposure and the O_3-corrected ERs were then defined as the y-intercept of the linear fit.

The methods used to calculate ERs are illustrated in Figure S.20 and Figure S.21. Figure S.20 shows acetylene, (m+p)-xylene and α-pinene mixing ratios against CO mixing ratios; marker shape is used to differentiate sampling time. The need for OH-correction is well illustrated by (m+p)-xylenes, for which the afternoon mixing ratios are lower than the morning and nighttime mixing ratios due to the relatively high reactivity with OH. The slope of the best linear fit using the nighttime data only is defined as the emission ratio (ER_{night}).[4] In Figure S.21, VOC/ΔCO for the same three compounds is plotted against OH exposure; the y-intercept of the best linear fit is defined as the emission ratio (OH-corrected ER). It can be seen that, as expected, α-pinene is not correlated with CO (Figure S.20) and the VOC/ΔCO shows no clear trend with OH exposure (Figure S.21).

Figure S.22 shows OH-corrected and O_3-corrected ERs vs. ERs_{night} (to both CO and acetylene). There is good agreement between the ERs calculated using the three different

approaches. Generally, the chemistry-corrected ERs are higher than the corresponding ERs_{night}. For highly reactive compounds, the chemistry-corrected ERs are expected to be higher. All ERs are reported in Table S.1.

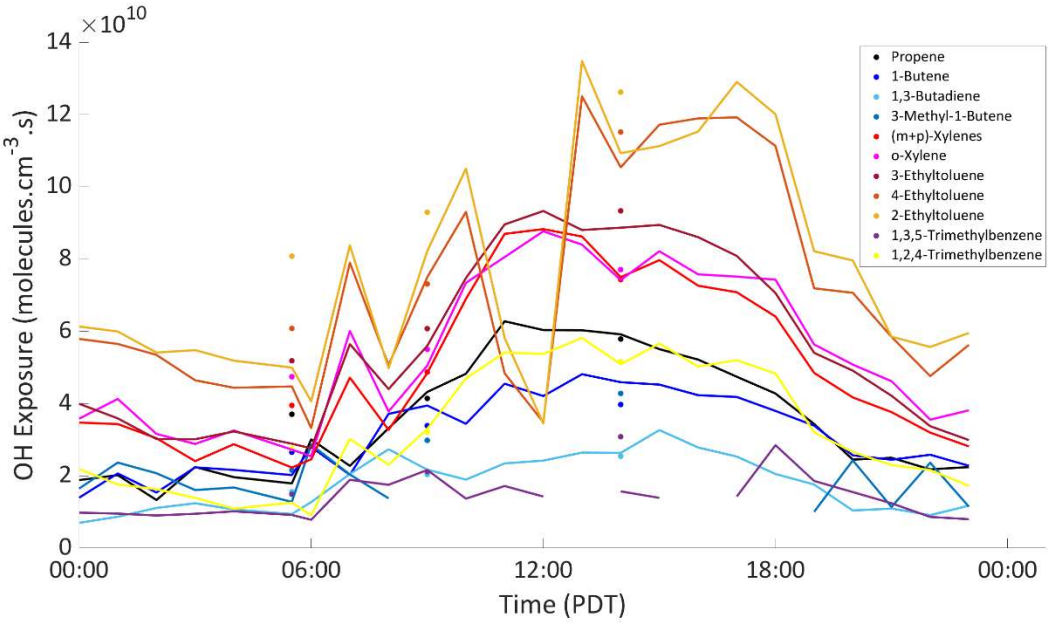

Figure S.18. OH-exposure calculated using the ratio of benzene to 11 more-reactive VOCs. Point markers represent OH-exposure calculated using the entire dataset (samples collected 3×/day). Lines represent OH-exposure calculated using two diurnal sample collections (one sample/hour for two 24-hour periods).

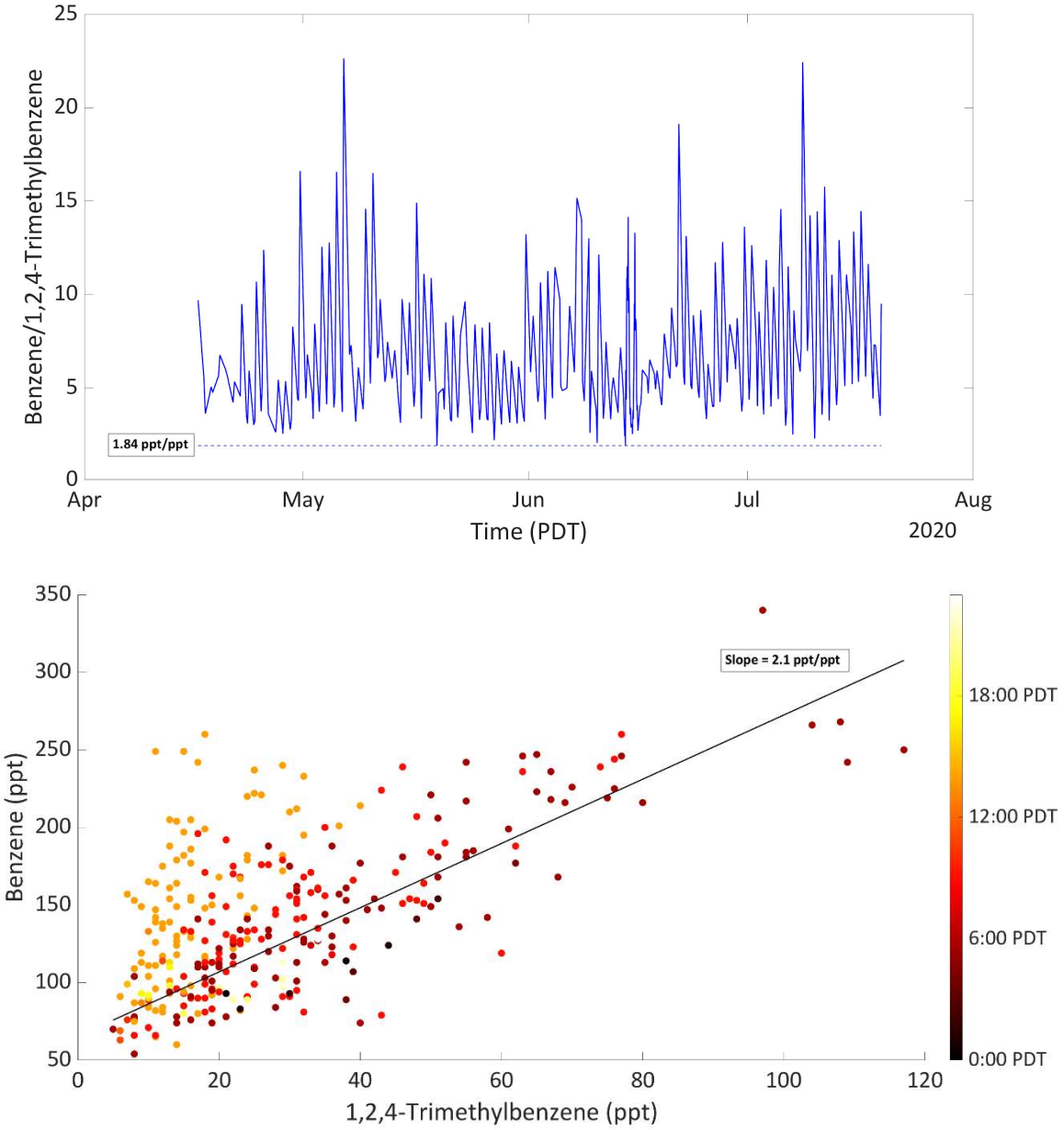

Figure S.19. Methods to determine the constant emission ratio of benzene:1,2,4-trimethylbenzene: time series of the ratio of measured benzene to measured 1,2,4-trimethylbenzene (top); and scatterplot of benzene and 1,2,4-trimethylbenzene mixing ratios (bottom). The dashed line in the top plot represents the lowest observed ratio (1.84 ppt/ppt). The

colors in the bottom plot are indicative of the time of day the sample was collected with dark colors representing nighttime and light colors representing afternoon.

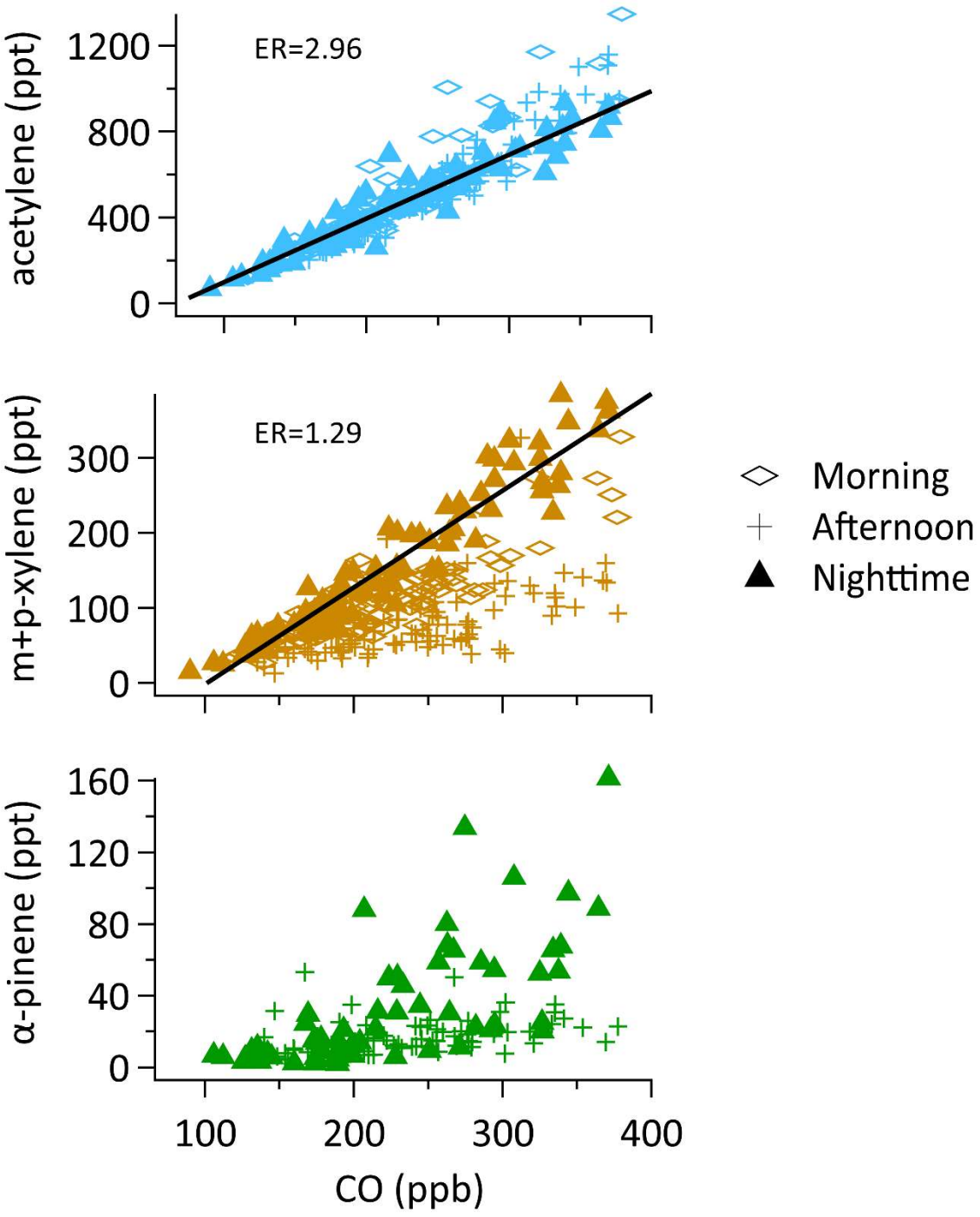

Figure S.20. Observed VOC versus CO mixing ratios for acetylene (blue), m+p-xylene (yellow), and α-pinene (green). Triangles indicate nighttime samples (05:30-06:30), diamonds indicate

morning samples (09:00-10:00), and + indicate afternoon samples (14:00-15:00). Emission ratios were calculated using the y-intercept of the linear fit for nighttime samples only. The α-pinene emission ratio was not calculated because of the poor correlation with CO.

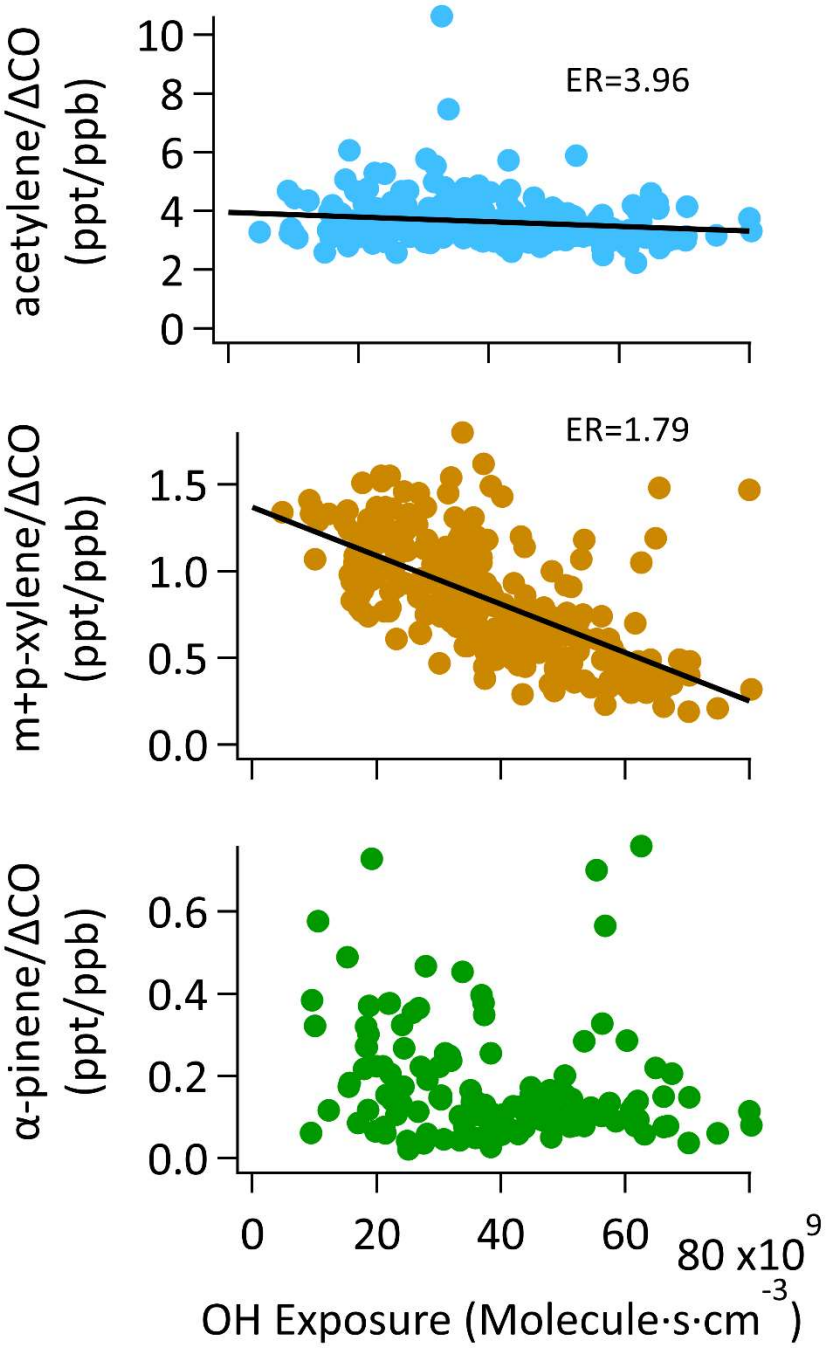

Figure S.21. Nighttime, morning, and afternoon VOC/ΔCO ratios versus calculated OH exposure for acetylene, m+p xylene, and α-pinene. The y-intercept is defined as the OH-corrected emission ratio.

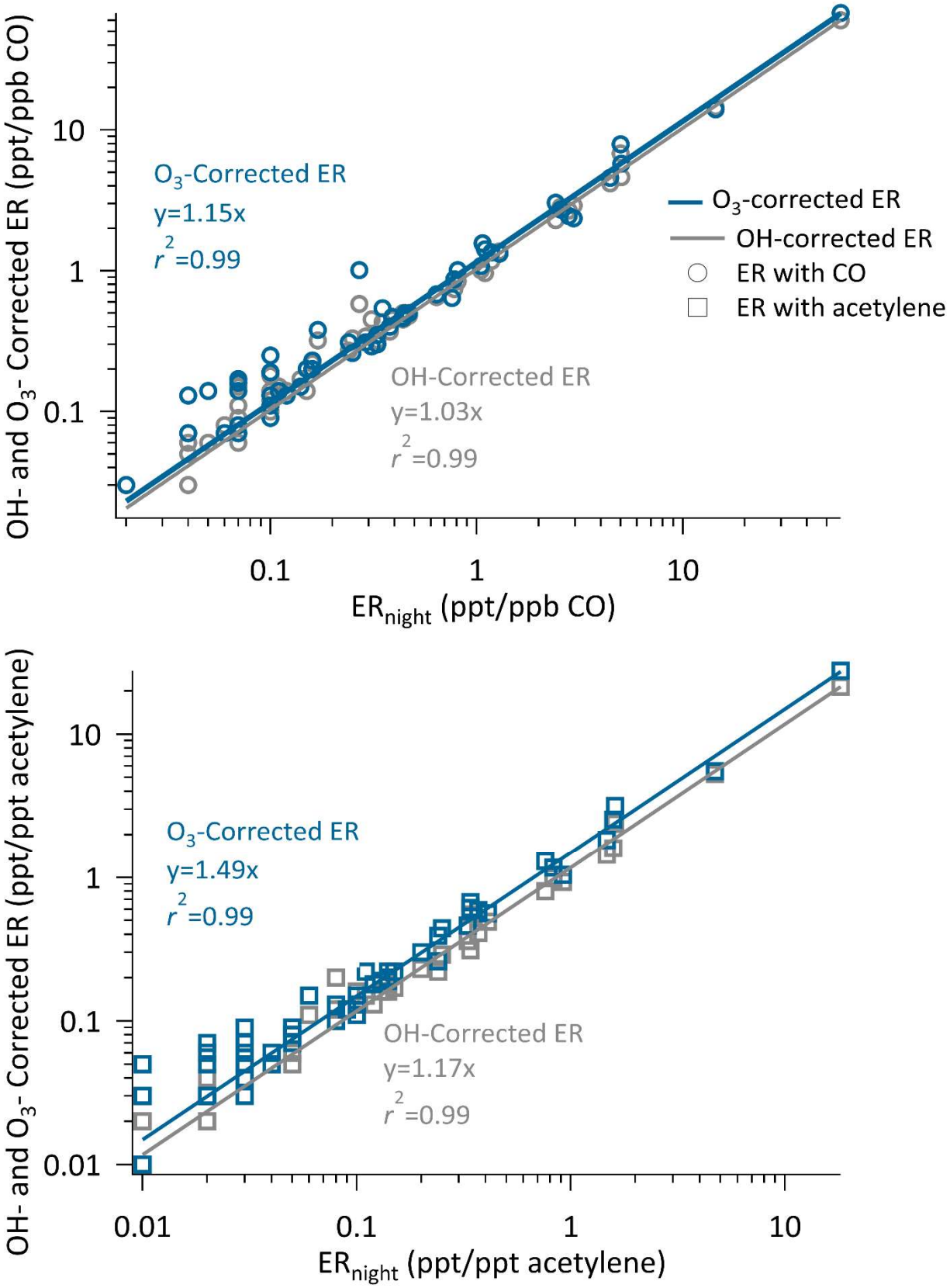
OH- and O3- Corrected ER (ppt/ppb CO)
10
1
0.1
O3-Corrected ER
y=1.15x
r2=0.99
O3-corrected ER
OH-corrected ER
ER with CO
ER with acetylene
OH-Corrected ER
y=1.03x
r2=0.99
0.1
1
10
ERnight (ppt/ppb CO)
OH- and O3- Corrected ER (ppt/ppt acetylene)
10
1
0.1
0.01
O3-Corrected ER
y=1.49x
r2=0.99
OH-Corrected ER
y=1.17x
r2=0.99
0.01
0.1
1
10
ERnight (ppt/ppt acetylene)

Figure S.22. OH- and O_3-corrected emission ratios plotted against nighttime emission ratios to CO (top) and acetylene (bottom). Slopes are reported for each of the four correlations with the intercept forced through zero.

S.4 Temperature Dependence of Terpene Emissions

Measured mixing ratios for six terpenes are plotted against temperature in Figure S.23. Three of the six terpenes, α-pinene, camphene, and eucalyptol appear to be more strongly correlated with temperature than the other three terpenes, β-myrcene, limonene, and ocimene.

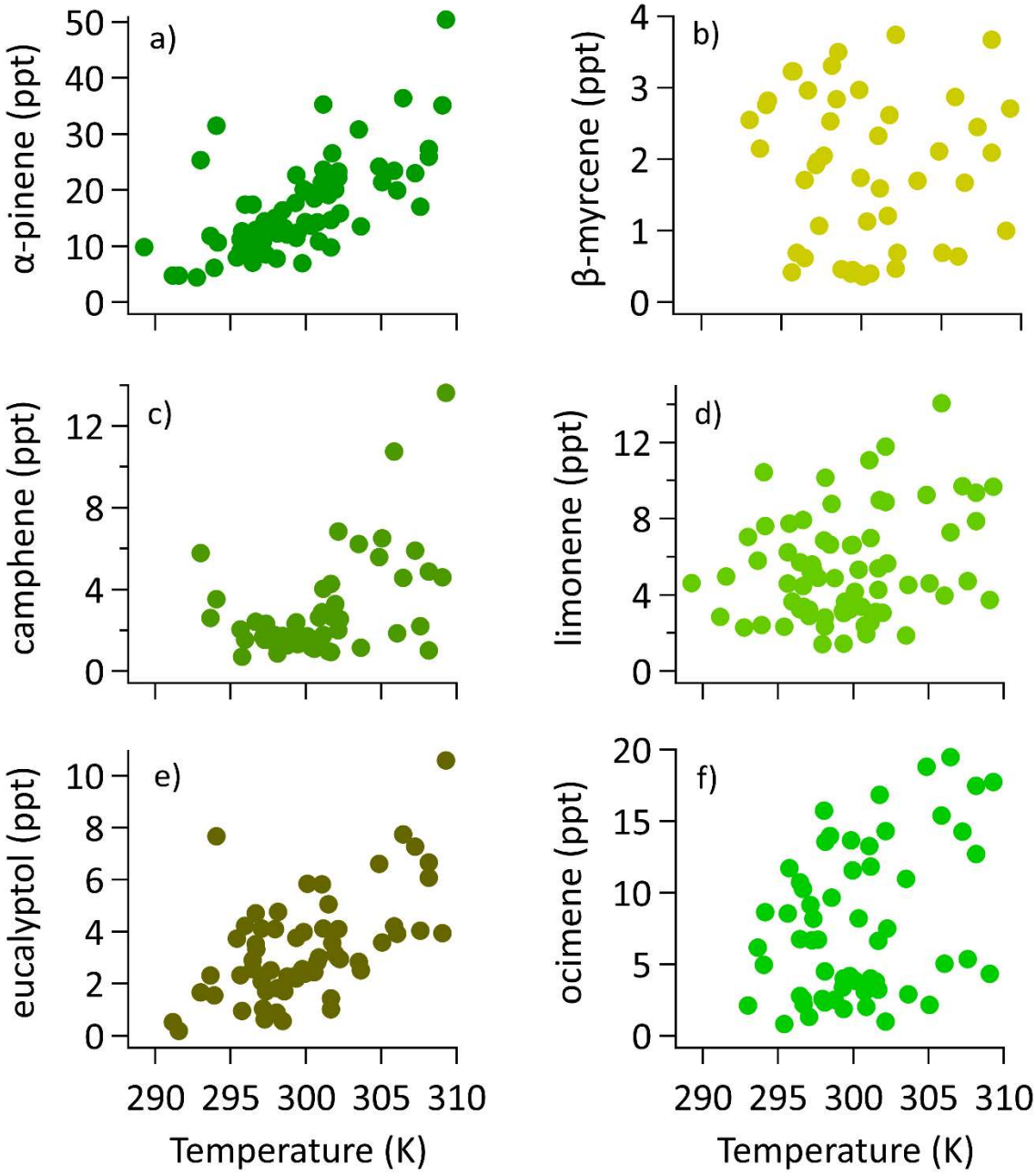

Figure S.23. Terpene mixing ratios plotted against temperature.

S.5 Trends in VOC Mixing ratios

The ratio of the June-July average mixing ratio to the April-May average mixing ratio is presented in Figure S.24 for 40 compounds; the compounds are ordered as in Table S.5. The

ratios for all compounds are close to one, supporting the conclusions that changes in human activity during LAAQC-2020 did not strongly affect the mixing ratios of this subset of compounds, which are largely combustion-derived VOCs.

To evaluate whether the 2020 combustion-derived VOC mixing ratios were anomalously low during the LAAQC sampling period, the average mixing ratios of three individual compounds (CO, acetylene, and i-pentane) and total non-methane hydrocarbons (NMHCs) measured during LAAQC-2020 were compared with average mixing ratios measured over the LA Basin during the NASA Student Airborne Research Program (SARP) between 2015-2019. The SARP data were averaged over a 5 year period to normalize differences in meteorology between years. The SARP data were collected onboard an aircraft at altitudes < 1 km. It is expected that the mixing ratios of the shorter-lived compounds would be lower in the samples collected aloft than those collected at the Pasadena ground site. For all three individual compounds (Figures S.25-S.27) and total NMHCs (Figure S.28), the median LAAQC values fall within the upper quartile of the SARP values.

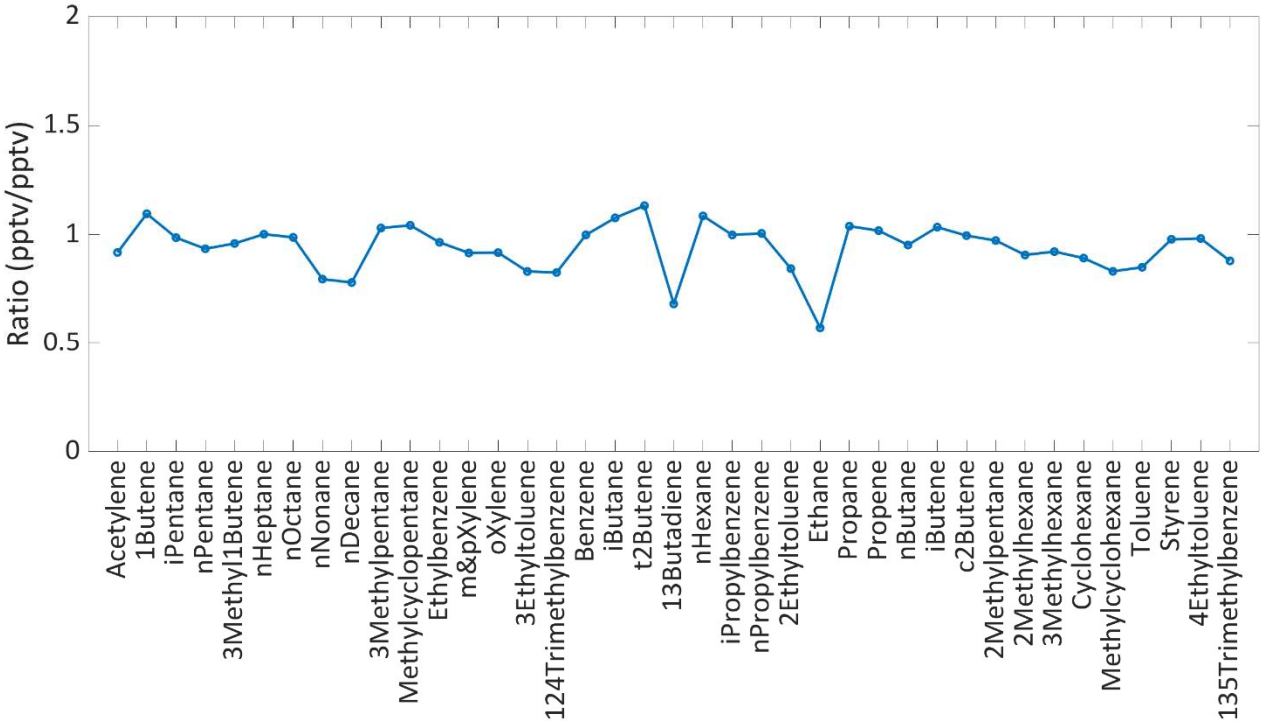

Figure S.24. The ratio of average June-July mixing ratio to average April-May mixing ratio for the 40 compounds listed in Table S.3.

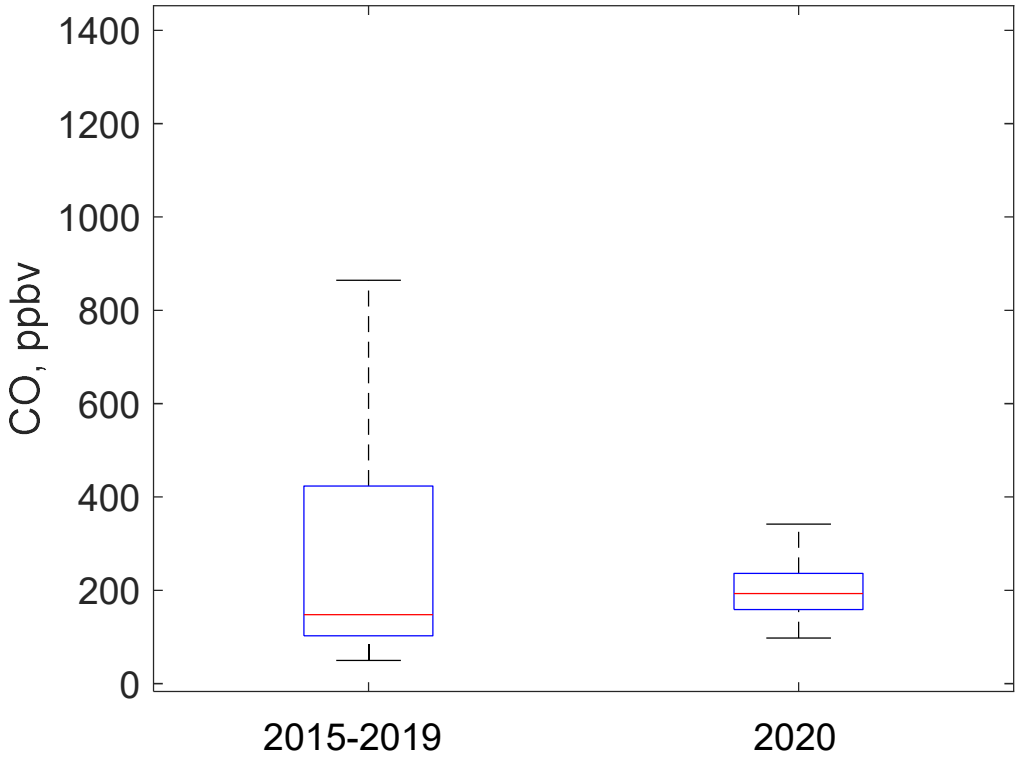

Figure S.25. Boxplots showing the CO mixing ratio measured as a part of SARP (2015-2019, left) and during LAAQC (2020, right). The median is represented by the red line and the 25th and 75th percentiles by the edges of the blue box.

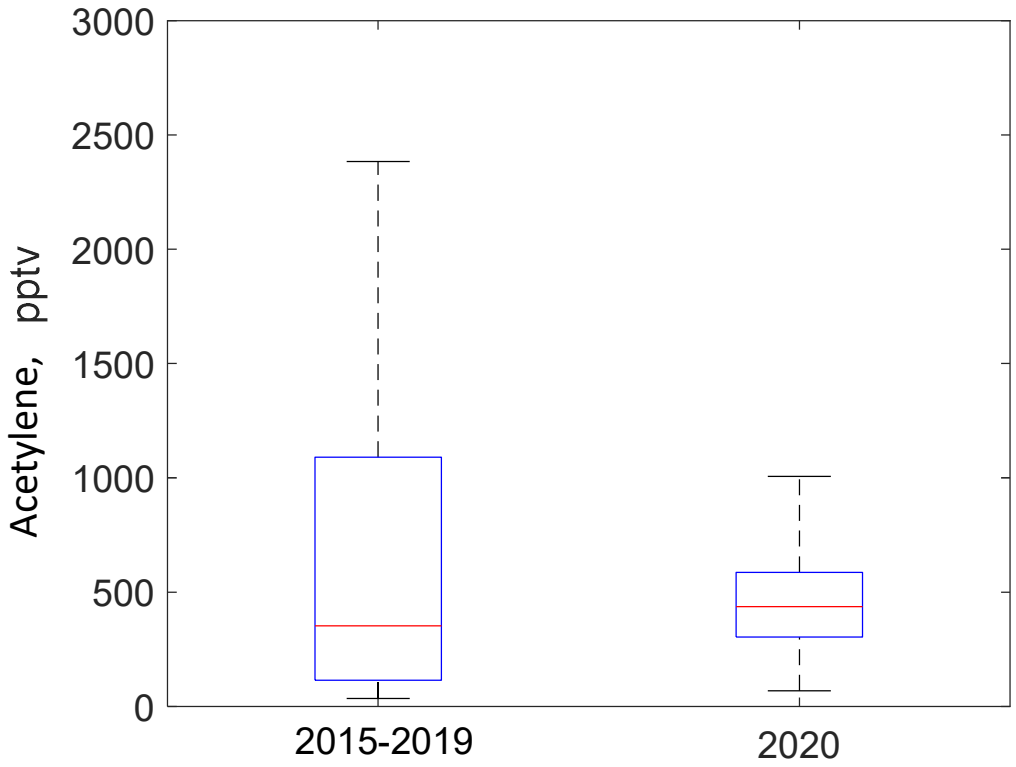

Figure S.26. Boxplots showing the acetylene mixing ratio measured as a part of SARP (2015-2019, left) and during LAAQC (2020, right). The median is represented by the red line and the 25th and 75th percentiles by the edges of the blue box.

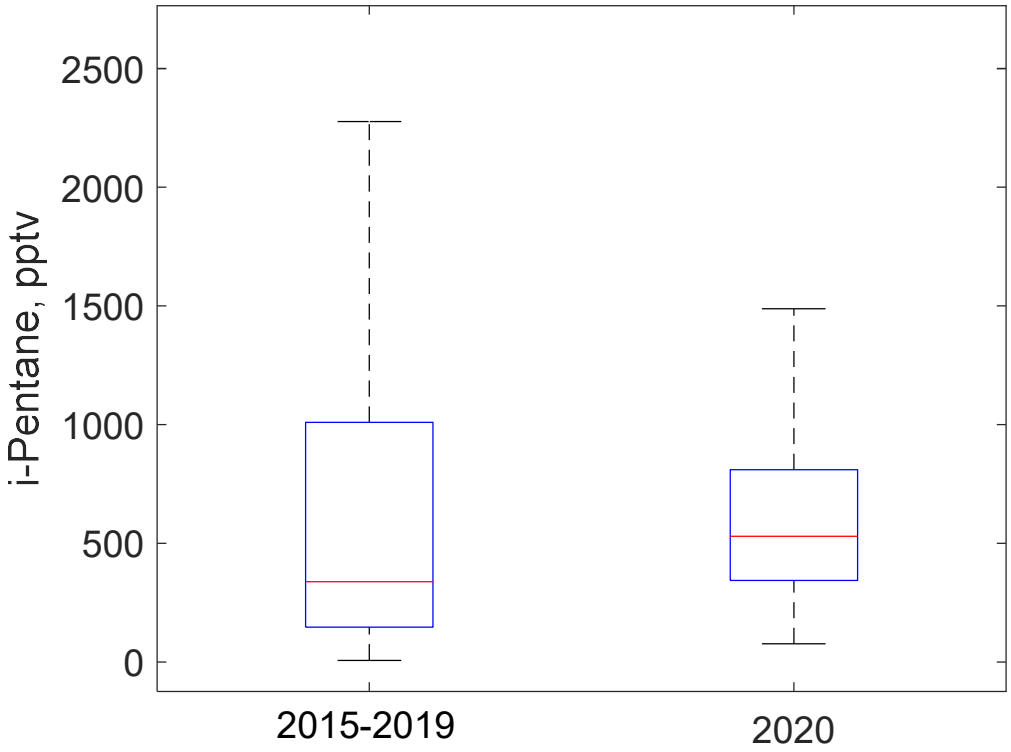

Figure S.27. Boxplots showing the i-pentane mixing ratio measured as a part of SARP (2015-2019, left) and during LAAQC (2020, right). The median is represented by the red line and the 25th and 75th percentiles by the edges of the blue box.

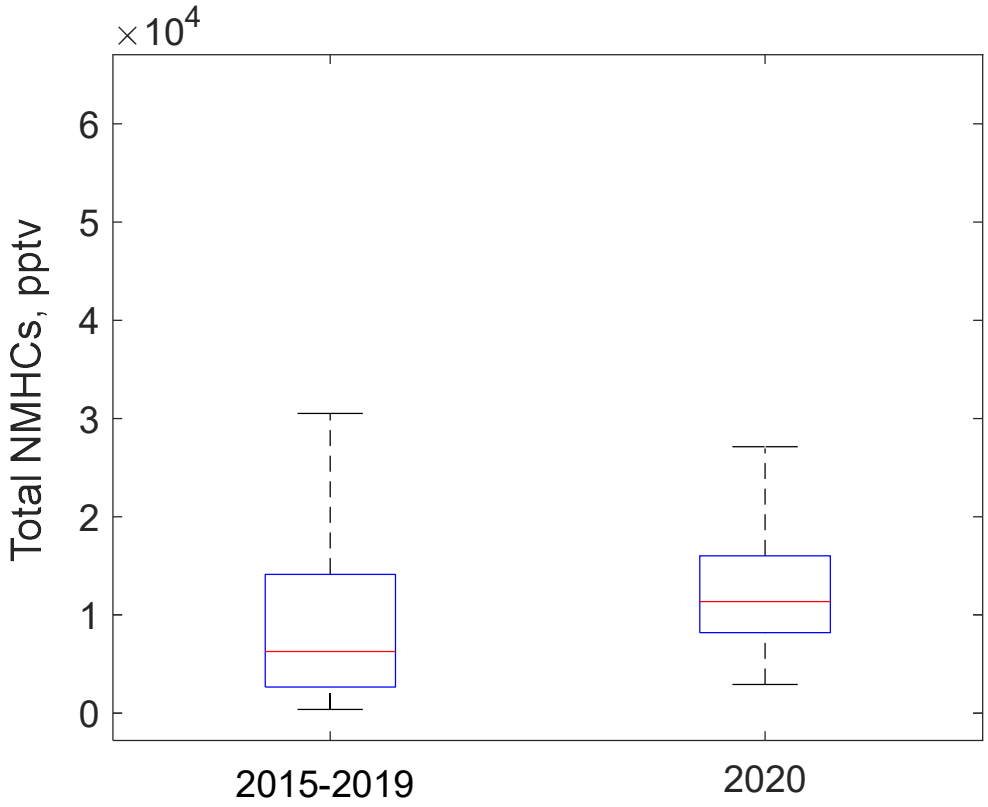

Figure S.28. Boxplots showing the total non-methane hydrocarbon (NMHC) mixing ratio measured as a part of SARP (2015-2019, left) and during LAAQC (2020, right). The median is represented by the red line and the 25th and 75th percentiles by the edges of the blue box.

References

(1) Parker, H. A.; Hasheminassab, S.; Crounse, J. D.; Roehl, C. M.; Wennberg, P. O. Impacts of Traffic Reductions Associated With COVID-19 on Southern California Air Quality. *Geophys. Res. Lett.* **2020**, *47* (23), e2020GL090164. https://doi.org/10.1029/2020GL090164.

(2) Stein, A.F., Draxler, R.R, Rolph, G.D., Stunder, B.J.B., Cohen, M.D., and Ngan, F. NOAA's HYSPLIT atmospheric transport and dispersion modeling system, *Bull. Amer. Meteor. Soc.* **2015**, 96 (12), 2059-2077. https://doi.org/10.1175/BAMS-D-14-00110.1.

(3) de Gouw, J. A. de; Gilman, J. B.; Kim, S.-W.; Lerner, B. M.; Isaacman-VanWertz, G.; McDonald, B. C.; Warneke, C.; Kuster, W. C.; Lefer, B. L.; Griffith, S. M.; Dusanter, S.; Stevens, P. S.; Stutz, J. Chemistry of Volatile Organic Compounds in the Los Angeles Basin: Nighttime Removal of Alkenes and Determination of Emission Ratios. *J. Geophys. Res. Atmospheres* **2017**, *122* (21), 11,843-11,861. https://doi.org/10.1002/2017JD027459.

(4) Atkinson, R.; Arey, J. Atmospheric Degradation of Volatile Organic Compounds. *Chem. Rev.* **2003**, *103* (12), 4605–4638. https://doi.org/10.1021/cr0206420.

(5) Borbon, A.; Gilman, J. B.; Kuster, W. C.; Grand, N.; Chevaillier, S.; Colomb, A.; Dolgorouky, C.; Gros, V.; Lopez, M.; Sarda-Esteve, R.; Holloway, J.; Stutz, J.; Petetin, H.; McKeen, S.; Beekmann, M.; Warneke, C.; Parrish, D. D.; Gouw, J. A. de. Emission Ratios of Anthropogenic Volatile Organic Compounds in Northern Mid-Latitude Megacities: Observations versus Emission Inventories in Los Angeles and Paris. *J. Geophys. Res. Atmospheres* **2013**, *118* (4), 2041–2057. https://doi.org/10.1002/jgrd.50059.

(6) Parrish, D. D., Stohl, A., Forster, C., Atlas, E. L., Blake, D. R., Goldan, P. D., Kuster, W. C., and de Gouw, J. A., Effects of mixing on evolution of hydrocarbon ratios in the troposphere, *J. Geophys. Res. Atmospheres* **2007**, *112*, D10S34. https://doi.org/10.1029/2006JD007583

(7) Hayes, P. L.; Ortega, A. M.; Cubison, M. J.; Froyd, K. D.; Zhao, Y.; Cliff, S. S.; Hu, W. W.; Toohey, D. W.; Flynn, J. H.; Lefer, B. L.; Grossberg, N.; Alvarez, S.; Rappenglück, B.; Taylor, J. W.; Allan, J. D.; Holloway, J. S.; Gilman, J. B.; Kuster, W. C.; Gouw, J. A. de; Massoli, P.; Zhang, X.; Liu, J.; Weber, R. J.; Corrigan, A. L.; Russell, L. M.; Isaacman, G.; Worton, D. R.; Kreisberg, N. M.; Goldstein, A. H.; Thalman, R.; Waxman, E. M.; Volkamer, R.; Lin, Y. H.; Surratt, J. D.; Kleindienst, T. E.; Offenberg, J. H.; Dusanter, S.; Griffith, S.; Stevens, P. S.; Brioude, J.; Angevine, W. M.; Jimenez, J. L. Organic Aerosol Composition and Sources in Pasadena, California, during the 2010 CalNex Campaign. *J. Geophys. Res. Atmospheres* **2013**, *118* (16), 9233–9257. https://doi.org/10.1002/jgrd.50530.